

# Non-constant geometric curvature for tailored spin-orbit coupling and chirality in superconductor-magnet heterostructures

Alv Johan Skarpeid,<sup>1,2</sup> Henning G. Hugdal,<sup>1</sup> Tancredi Salamone,<sup>1</sup> Morten Amundsen,<sup>1,3</sup> and Sol H. Jacobsen<sup>1,\*</sup>

<sup>1</sup>*Center for Quantum Spintronics, Department of Physics, NTNU,*

*Norwegian University of Science and Technology, NO-7491 Trondheim, Norway*

<sup>2</sup>*Department of Physics, Centre for Materials Science and Nanotechnology, University of Oslo, NO-0316 Oslo, Norway*

<sup>3</sup>*Nordita, KTH Royal Institute of Technology and Stockholm University,*

*Hannes Alfvéns väg 12, SE-106 91 Stockholm, Sweden*

(Dated: April 11, 2024)

We show that tailoring the geometric curvature profile of magnets can be used for bespoke design of an effective non-relativistic spin-orbit coupling, which may be used to control proximity effects if the magnet is coupled to a superconductor. We consider proximity-coupled one-dimensional magnetic wires with variable curvatures, specifically three distinct shapes classified as J-, C-, and S-type. We demonstrate a chirality-dependent spin polarization of the superconducting correlations, and show the role of curvature in determining the ground state of mixed-chirality junctions. We speculate on how this may be implemented in novel device design, and include analysis of its usage in a spin-triplet SQUID.

## I. INTRODUCTION

Combining the typically competing phases of superconductivity and magnetism provides fertile ground for uncovering fundamental physics, and is essential for advancing the field of superconducting spintronics<sup>1,2</sup>. Resistance-free spin and charge transport in superconductors can give an energy advantage in spintronics, where high current densities are needed for novel information processing architectures. However, there are a limited number of combination mechanisms, and strong restrictions on the tailoring and control of these. Geometric curvature has recently emerged as providing a range of new freedoms for design and control<sup>3-5</sup>, and here we examine the implications of non-constant curvatures in magnets coupled to superconductors.

The most abundant superconductors are robust to impurities, with conventional, singlet, s-wave orbital correlations (Cooper pairs), where averaging over scattering events in momentum-space leaves a finite superconducting order parameter. However, singlet pairs are rapidly destroyed in a spin-polarized material such as a ferromagnet. To combine diffusive s-wave, singlet superconductivity with magnetism, we instead need to convert the singlet pairings into odd-frequency<sup>6</sup> spin-polarized triplets. This is done via the proximity effect, where properties of adjacent materials merge through their interfacial barriers<sup>7-9</sup>. Traditionally, the conversion is manufactured via magnetic inhomogeneities, such as misaligned magnetic multilayers or an intrinsically helical magnetic lattice structure<sup>10-12</sup>, or via intrinsic spin-orbit coupling (SOC)<sup>13-15</sup>. However, manipulating individual magnetic multilayers can be challenging experimentally, and helical spin lattice textures are fixed, and cannot be varied or tailored. Moreover, intrinsic SOC is a relativistic effect, dependent on non-centrosymmetric crystal structures and/or spatially restricted interfacial symmetry breaking, so options for tailoring and controlling such systems are rather limited.

In contrast, curvature in real-space (as opposed to the related field of band-structure curvature) can be a source of non-relativistic spin orbit effects in magnetic systems, which we have shown can be harnessed to tailor and control diffusive proximity effects for combining superconductivity and magnetism<sup>4,5,16</sup>. For instance, curvature can control the direction of charge current flow through a Josephson junction<sup>16</sup>, it can act as a probe of the quality of an uncompensated antiferromagnetic interface<sup>5</sup>, or even control the superconducting transition itself<sup>4</sup>.

Research into the role of curvature has increased dramatically in recent years<sup>3</sup>, for example showing interesting effects in semiconductors<sup>17-21</sup> and in superconductors<sup>22-25</sup>. The curvature can for example promote topological edge states<sup>18</sup> and topological superconductivity<sup>25</sup>. Curvature induces a quantum geometric potential<sup>26-29</sup>, and may induce a strain field producing a curvature-induced Rashba-type spin-orbit coupling<sup>30-33</sup>. If a material is magnetic, Rashba SOC leads to a chiral or extrinsic Dzyaloshinskii-Moriya interaction (DMI) and magnetic anisotropy<sup>34-40</sup>, and it is the curvature-controlled rotation of the spin orientation axis that is the source of non-relativistic spin-orbit effects in magnets<sup>4,5,16</sup>. Curvature-induced DMI can cause the appearance of chiral and topological spin textures of the effective magnetization in toroidal nanomagnets<sup>41,42</sup>, bent nanotubes<sup>43,44</sup>, curved surfaces<sup>45</sup>, nanohelices<sup>46,47</sup> and spherical shells<sup>40,48,49</sup>.

Materials design and fabrication of nanostructures with curved geometries has also been rapidly advancing to create ever smaller and more intricate nanoscale designs, from etching<sup>50,51</sup> and compressive buckling<sup>52</sup>, to electron beam lithography<sup>53-55</sup>, two-photon lithography<sup>56,57</sup>, glancing angle deposition<sup>58</sup> and focused electron beam induced deposition<sup>59,60</sup>. The curved designs can be manipulated in situ via strain, with dynamical control via photostriction, piezoelectrics, thermoelectric effects, tuning of the surface chemistry and more<sup>61-63</sup>.

In this article, we investigate non-constant curvature

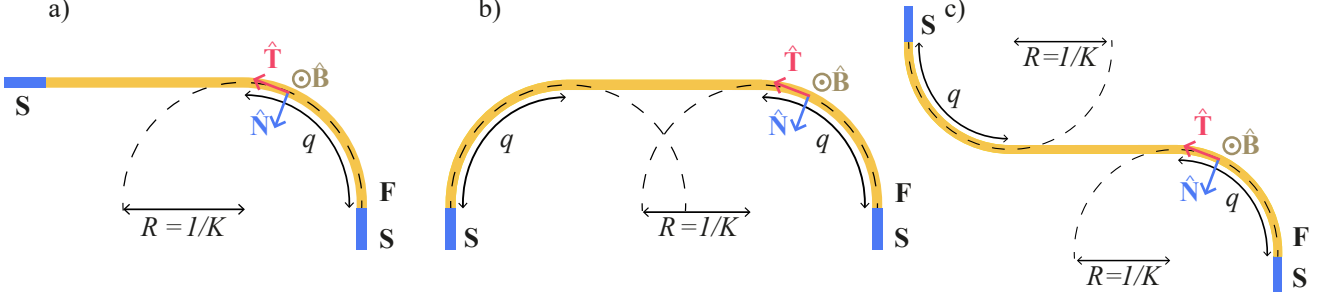


FIG. 1. The (a) J-, (b) C- and (c) S-type superconductor-ferromagnet-superconductor (SFS) junction. The three orthonormal basis vectors  $\hat{T}(s)$ ,  $\hat{N}(s)$  and  $\hat{B}(s)$  are indicated in (a). Here,  $q$  is the parameter indicating the length of the curved section(s) and  $K > 0$  the curvature amplitude of the curved sections; a segment with curvature amplitude  $K$  follows a circular arc of radius  $R = 1/K$ .

in three classes of magnetic nanowires (J-, C- and S-type; see Fig. 1), and demonstrate how such variable curvatures can influence the proximity effect and spintronic device design. We show a chirality-dependent spin polarization, investigate the ground state in mixed-chirality junctions, and we discuss this in the context of a spin-triplet SQUID design.

## II. THEORY

In Sec. II A, we introduce the quasiclassical Usadel equation of motion and relevant boundary conditions for diffusive spin transport, generalized to curved heterostructures. In Sec. II B we present the parameterisation of curves with non-constant curvature that define the classes of curves (J, C, and S) presented in Fig. 1. The numerical approach for solving the spin transport equations via Riccati parameterisation is summarized in Sec. II C.

### A. Quasiclassical formalism: Usadel equation in curvilinear coordinates

We employ the quasiclassical formalism<sup>64,65</sup> where observables are retrievable from a propagator  $\check{g}$  in Keldysh  $\otimes$  Nambu (particle-hole)  $\otimes$  spin space,

$$\check{g} = \begin{pmatrix} \hat{g}^R & \hat{g}^K \\ 0 & \hat{g}^A \end{pmatrix}, \quad (1)$$

where the superscripts  $R$ ,  $A$  and  $K$  label the retarded, advanced and Keldysh components, respectively. The elements are related by  $\hat{g}^A = -\hat{\tau}_3 \hat{g}^{R\dagger} \hat{\tau}_3$  and  $\hat{g}^K = \hat{g}^R \hat{h} - \hat{h} \hat{g}^A$ , where we refer to  $\hat{h}$  as the *distribution matrix* and  $\hat{\tau}_3 = \text{diag}(1, 1, -1, -1)$ .

The propagator  $\check{g}$  obeys the Usadel equation<sup>65</sup>, which in curvilinear coordinates is given as<sup>4</sup>

$$D_F G^{\mu\nu} \tilde{D}_\mu \left( \check{g} \tilde{D}_\nu \check{g} \right) + i \left[ \epsilon \hat{\tau}_3 \otimes I_2 + \check{\Sigma}, \check{g} \right] = 0, \quad (2)$$

where  $D_F$  is the diffusion coefficient,  $\epsilon$  is the energy,  $\check{\Sigma}$  is the self-energy function,  $G^{\mu\nu}$  is the metric tensor, and  $I_2$  is the  $2 \times 2$  identity matrix in Keldysh space. The coordinate-gauge covariant derivatives are given as

$$\tilde{D}_\mu v_\nu = \tilde{\partial}_\mu v_\nu - \Gamma_{\mu\nu}^\gamma v_\gamma, \quad (3)$$

with Christoffel symbols

$$\Gamma_{\mu\nu}^\gamma = \frac{1}{2} G^{\gamma\lambda} [\partial_\nu G_{\mu\lambda} + \partial_\mu G_{\lambda\nu} - \partial_\lambda G_{\mu\nu}], \quad (4)$$

and gauge-only covariant derivative  $\tilde{\partial}_\mu v_\nu = \partial_\mu v_\nu - i[\hat{A}_\mu, v_\nu]$ . The gauge field  $\hat{A}_\mu = \text{diag}(A_\mu, -A_\mu^*)$  will depend on e.g. intrinsic SOC contributions.

The Christoffel symbols depend on the choice of coordinate system, and we consider a planar space curve in real, 3-dimensional space,  $\mathbf{r}(s)$ , at the center of a ferromagnetic nanowire. This space, and the nanowire, is parametrizable as  $\mathbf{R}(s, n, b) = \mathbf{r}(s) + n\hat{N}(s) + b\hat{B}(s)$ , where we refer to  $s$ ,  $n$  and  $b$  as the *arclength*, *normal* and *binormal coordinates* respectively. The orthonormal basis vectors for the parametrization are  $\hat{T}(s) = \partial_s \mathbf{r}(s)$ ,  $\hat{N}(s) = \partial_s \hat{T}(s) / \kappa(s)$ , and  $\hat{B}(s) = \hat{T}(s) \times \hat{N}(s)$ , which correspond to the *tangential*, *normal* and *binormal* direction as illustrated in Fig. 1. We refer to  $\kappa(s)$  as the *curvature function*.

The basis vectors obey a Frenet-Serret like equation

$$\begin{pmatrix} \partial_s \hat{T}(s) \\ \partial_s \hat{N}(s) \\ \partial_s \hat{B}(s) \end{pmatrix} = \begin{pmatrix} 0 & \kappa(s) & 0 \\ -\kappa(s) & 0 & 0 \\ 0 & 0 & 0 \end{pmatrix} \begin{pmatrix} \hat{T}(s) \\ \hat{N}(s) \\ \hat{B}(s) \end{pmatrix}, \quad (5)$$

and are accompanied by a non-trivial metric tensor<sup>4,66</sup>  $G_{\mu\nu} = \text{diag}(\eta^2, 1, 1)$ , with  $\eta(s, n) = 1 - \kappa(s)n$ . When the system is in equilibrium, it is sufficient to consider only the retarded propagator,  $\hat{g}^R$ . Moreover, in the 1D transport limit, where  $n, b \rightarrow 0$  with  $\partial_s \kappa(s)$  finite, the non-zero Christoffel symbols do not contribute to the Usadel equation, and the basis vectors remain orthonormal, such

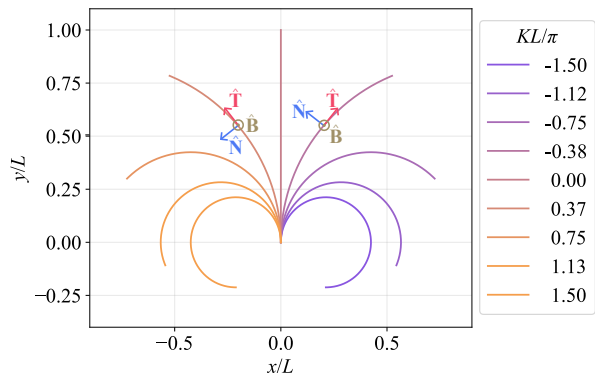


FIG. 2. Lines of constant curvature as a function of the curvature amplitude  $K$ . Changing the sign of  $K$  from positive to negative reverses the direction of the curvature from anti-clockwise to clockwise. The basis vectors, as given in Eqn. 10, are drawn for two of the curves.

that the Usadel equation for the retarded propagator takes the form<sup>4</sup>

$$D_F \tilde{\partial}_s (\hat{g}^R \tilde{\partial}_s \hat{g}^R) + i \left[ \epsilon \hat{\tau}_3 + \hat{\Sigma}, \hat{g}^R \right] = 0. \quad (6)$$

In this form, the effect of the curvature is encoded in the rotation of the basis vectors (and Pauli matrices) along the arclength.

Considering a superconductor/ferromagnet heterostructure, we take the self-energy  $\hat{\Sigma} = \hat{\Delta}$  on the superconducting side, and  $\hat{\Sigma} = h^\mu(s) \text{diag} [\sigma_\mu(s), \sigma_\mu^*(s)]$  on the ferromagnetic side.  $h^\mu(s)$  is the exchange field and  $\sigma_\mu(s)$  the Pauli matrices along the  $\mu$ -direction, and  $\hat{\Delta} = \text{antidiag}(\Delta, -\Delta, \Delta^*, -\Delta^*)$ , where  $\Delta$  is the superconducting order parameter. In the following, we keep  $\Delta$  fixed and equal to its value in an infinite superconductor, thereby ignoring the inverse proximity effect caused by the interface. All lengths are scaled relative to the diffusive superconducting coherence length, denoted by  $\xi$ , which is typically of the order of a few tens of nanometers.

For the boundary conditions we will employ the Kupryanov-Lukichev boundary conditions<sup>67</sup>, which take the form

$$\check{g}_j \tilde{\partial}_I \check{g}_j = \frac{1}{2L_j \zeta_j} [\check{g}_L, \check{g}_R], \quad (7)$$

where the index  $j = \{L, R\}$  refers to the left and right side of the interface,  $L_j$  is the length of material,  $\tilde{\partial}_I$  is the gauge covariant derivative at the interface, and  $\zeta_j = R_B/R_j$  quantifies the interfacial resistance via the ratio of barrier resistance  $R_B$  to bulk resistance  $R_j$ .

### B. Parametrization of non-constant, step-like curvature functions

We consider junctions consisting of straight and curved parts in series. Mathematically, this is done by considering curvature functions,  $\kappa(s)$ , consisting of a series

of step-functions, as opposed to constants for constant curvature<sup>4,16</sup>. We will demonstrate that approximate step-functions can be rigorously included in the formalism and use them to define the J-, C- and S-classes of curves.

We will consider planar curves that can be parameterized using curvature functions of the form

$$\kappa(s) = K \sum_j \alpha_j H(s - q_j), \quad (8)$$

where we refer to  $K$  as the *curvature amplitude*, and  $H$  is the Heaviside step function. Particular values from the sets  $\{q_j\}$  and  $\alpha_j = \pm 1$  determine where the curvature is present and/or reversed. The orientation of the unit vectors relative to their initial configuration,  $\theta(s)$ , can then be determined from the integral of the curvature function  $\kappa(s)$ :

$$\begin{aligned} \theta(s) &= \int_{\lambda=0}^{\lambda=s} \kappa(\lambda; K, q) d\lambda \\ &= K \sum_j \alpha_j H(s - q_j) \cdot (s - q_j), \end{aligned} \quad (9)$$

such that we may parameterize the basis vectors as

$$\hat{T}(s) = -\sin \theta(s) \hat{x} + \cos \theta(s) \hat{y}, \quad (10a)$$

$$\hat{N}(s) = -\cos \theta(s) \hat{x} - \sin \theta(s) \hat{y} \quad (10b)$$

$$\hat{B}(s) = \hat{z}. \quad (10c)$$

The conceptually simple case of constant curvature, with  $\kappa(s) = K$ , is shown in Fig. 2. When we have fixed the binormal basis vector,  $\hat{B}(s)$ , positive (negative) curvature functions  $\kappa(s)$  correspond to counter-clockwise (clockwise) rotation.

For this demonstration of non-constant curvature, we consider three conceptually simple cases: wires curved at one end (J-type), curved in the same direction at each end (C-type), or curved in opposite directions on each end (S-type), as shown in Fig. 1. The associated curvature functions are

$$\kappa^J(s; K, q) = KH(s - q), \quad (11a)$$

$$\kappa^C(s; K, q) = \begin{cases} K & \text{if } s < q \\ 0 & \text{if } q < s < L - q \\ K & \text{otherwise,} \end{cases} \quad (11b)$$

$$\kappa^S(s; K, q) = \begin{cases} K & \text{if } s < q \\ 0 & \text{if } q < s < L - q \\ -K & \text{otherwise.} \end{cases} \quad (11c)$$

Using Eq. (9), this gives

$$\theta^J(s; K, q) = \begin{cases} Ks & \text{if } s < q \\ Kq & \text{otherwise,} \end{cases} \quad (12a)$$

$$\theta^C(s; K, q) = \begin{cases} Ks & \text{if } s < q \\ Kq & \text{if } q < s < L - q \\ K(s+2q-L) & \text{otherwise,} \end{cases} \quad (12b)$$

$$\theta^S(s; K, q) = \begin{cases} Ks & \text{if } s < q \\ Kq & \text{if } q < s < L - q \\ K(L - s) & \text{otherwise.} \end{cases} \quad (12c)$$

Here  $L$  is the length of the parameterized section, and we refer to  $q$  as the *shape parameter*.

To ensure continuously varying observables, and to rigorously derive the Usadel equation in 1D, we require a continuous  $\kappa(s)$  and finite  $\partial_s \kappa(s)$ . To achieve this we may approximate the Heaviside function by the hyperbolic tangent, and thus the curvature functions may, as an example, take the form

$$\kappa^J(s; K, a, q) = K \left( 1 - \frac{e^{a(s-q)}}{1 + e^{a(s-q)}} \right). \quad (13)$$

Here we have defined a *sharpness parameter*  $a$ , indicating the abruptness of the change in curvature. In the limit  $a \rightarrow \infty$  we retrieve the step-function, giving Eq. (11). We may further insert Eq. (13) into Eq. (9), to get

$$\theta^J(s; K, a, q) = K \left[ s + \frac{1}{a} \ln \left( \frac{1 + e^{-aq}}{1 + e^{a(s-q)}} \right) \right]. \quad (14)$$

There are closed form expressions for  $\theta^{S,C}$ , as well as for more generalized cases. There is, however, in general no closed form expression for the parameterized curve itself.

### C. Numerical approach: Riccati parametrization

To numerically solve Eq. (6), it is helpful to employ a more tractable parameterization of the quasiclassical Green's function. We use the Riccati parametrization<sup>15,68</sup>:

$$\hat{g}^R = \begin{pmatrix} N(1 + \tilde{\gamma}) & 2N\tilde{\gamma} \\ -2\tilde{N}\tilde{\gamma} & -\tilde{N}(1 + \tilde{\gamma}) \end{pmatrix}, \quad (15)$$

with  $N = (1 - \gamma\tilde{\gamma})^{-1}$  and  $\tilde{\gamma}(s, \varepsilon) = \gamma^*(s, -\varepsilon)$ , i.e. tilde-conjugation implies inversion of the quasiparticle energy and element wise complex conjugation. The parametrization reduces the dimensionality of the problem from an equation of  $(4 \times 4)$ -matrices to coupled equations for  $(2 \times 2)$ -matrices, and bounds the norm of the matrix elements  $\in [0, 1]$ .

In the ferromagnetic region, the Usadel equation is then parametrized as

$$D_F \left\{ \partial_s \gamma + 2(\partial_s \gamma) \tilde{N} \tilde{\gamma} (\partial_s \gamma) \right\} = -2i\varepsilon\gamma - ih^\mu [\sigma_\mu(s) \gamma - \gamma \sigma_\mu^*(s)], \quad (16)$$

with the index  $\mu = \{\hat{T}, \hat{N}, \hat{B}\}$ , and  $\sigma_\mu(s)$  are the corresponding Pauli matrices. The unit vectors  $\hat{T}(s), \hat{N}(s), \hat{B}(s)$  are determined from Eq. (10) with  $\theta(s)$  being, e.g., Eq. (14) for a J-type curve or Eq. (12b) for a C-type curve. Inserting the Riccati parametrization Eq. (15) into the boundary conditions Eq. (7) at the superconductor-ferromagnet interface, the boundary conditions for the matrix  $\gamma$  become<sup>4,15</sup>:

$$\tilde{\partial}_I \gamma_S = \frac{1}{L_S \zeta_S} (1 - \gamma_S \tilde{\gamma}_F) N_F (\gamma_F - \gamma_S), \quad (17a)$$

$$\tilde{\partial}_I \gamma_F = \frac{1}{L_F \zeta_F} (1 - \gamma_F \tilde{\gamma}_S) N_S (\gamma_F - \gamma_S). \quad (17b)$$

The corresponding equations for  $\tilde{\gamma}$  are obtained by tilde conjugation of Eqs. (16) to (17).

We can then solve the complete, Riccati parameterized Usadel equation (16) in a 1D ferromagnetic region with either constant or non-constant curvature functions, coupled to bulk  $s$ -wave superconductors, employing the Kupriyanov-Lukichev boundary conditions (17) at the interfaces. The specific implementation is based on<sup>69</sup>, modified to accommodate the non-constant curvature as specified here, and run using the `bvp6c` package for MATLAB.

## III. RESULTS

We begin by examining the Usadel equations in the limit of weak proximity coupling in Sec. III A, where we can get analytic insight into the dominant mechanisms influencing the spin transport. We discuss this analytic insight in the context of the simpler J-type curve in Sec. III B. We then present numerical results for the full proximity effect in C- and S-type junctions. In particular, we show a chirality-dependent switch in the magnetization and spin current density of C-type curves in Sec. III C 1. We compare the equilibrium current of C- and S-type curves in Sec. III C 2, and show that only C-type undergo a  $0 - \pi$  transition, since the combination of *equal* chiralities in an S-type junction interferes destructively.

### A. Weak proximity equations

In the weak proximity limit, we assume the anomalous Green's function to be small, such that

$$\hat{g}^R = \begin{pmatrix} 1 & f \\ -\tilde{f} & 1 \end{pmatrix}, \quad (18)$$

and parametrize the anomalous Green's function using the d-vector formalism:

$$f = (f_0 + d_\mu \sigma_\mu) i \sigma_y. \quad (19)$$

Here  $f_0$  and  $d_\mu$  are the singlet and triplet amplitudes respectively. In this limit, we need only to consider the

terms of the Riccati parametrized equation that are linear in  $\gamma$ , and the equation takes the following form in the ferromagnetic region:

$$\frac{iD_F}{2}\partial_s^2 f_0 = \varepsilon f_0 + h_\mu d_\mu, \quad (20a)$$

$$\frac{iD_F}{2}\partial_s^2 d_T - iD_F(\partial_s \kappa + \kappa \partial_s) d_N = \left[ \varepsilon + \frac{iD_F \kappa^2}{2} \right] d_T + h_T f_0, \quad (20b)$$

$$\frac{iD_F}{2}\partial_s^2 d_N + iD_F(\partial_s \kappa + \kappa \partial_s) d_T = \left[ \varepsilon + \frac{iD_F \kappa^2}{2} \right] d_N + h_N f_0, \quad (20c)$$

$$\frac{iD_F}{2}\partial_s^2 d_B = \varepsilon h_B + h_B f_0. \quad (20d)$$

With a non-zero  $\kappa$ , the triplet components undergo spin precession and spin relaxation. We identify the precession with the terms having a first order derivative, while the imaginary contributions to the energy represent the spin relaxation and loss of spin information from impurity scattering. While the curvature  $\kappa(s)$  provides a mechanism for rotating between different triplet components, generating the spin-polarized triplets that are robust in magnetic fields (the so-called long-ranged component), it also induces spin relaxation. Having a non-constant curvature function,  $\kappa(s)$ , enables optimization of the long-range triplet generation and retention.

The triplet component with zero spin projection is short-ranged in a magnet, with d-vector parallel to the exchange field; the triplet component with spin polarization along the exchange field is long-ranged, with a d-vector perpendicular to the exchange field. For example, if the exchange field is directed along  $\hat{T}$ , the short-ranged triplets can be identified with  $d_T$ , while  $d_N$  and  $d_B$  are long ranged.

In the weak proximity equations, we can see a curvature dependent mixing between  $d_N$  and  $d_T$ . The mixing depends on  $\partial_s \kappa$ , which couples to the amplitudes themselves,  $d_\mu$ , rather than their derivatives. That is, the mixing is enhanced in regions where the curvature changes abruptly. Moreover, it is possible to change the sign of  $\partial_s \kappa$  without changing that of  $\kappa$ .

### B. J-type ferromagnets and chirality-dependent spin polarization

The simplest class of wires with non-constant curvature is the J-type ferromagnet (see Fig. 1(a) and Fig. 3). For any superconductor-ferromagnet (SF) bilayer, the ferromagnet's exchange field will convert a proportion of the superconducting singlet correlations into triplets with non-zero spin projection (short-ranged triplets), which is clear from Eq. (20). The curvature is then responsible for the rotation of the triplet vector, converting between triplets with and without spin projection. Since the short ranged triplet correlations decay rapidly in a

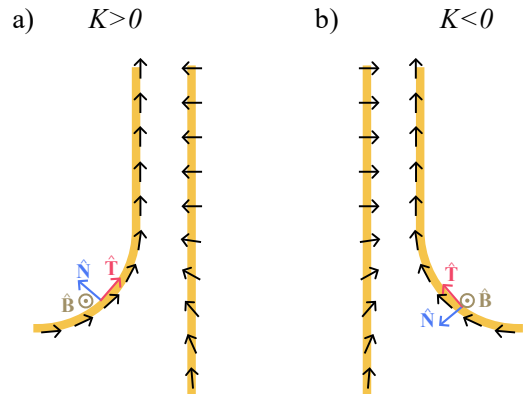


FIG. 3. Illustration of the exchange field, i.e. the tangent vectors, for a J-like curve at equidistant points along the curve for (a)  $K > 0$  and (b)  $K < 0$ . An equivalent system with a straight wire and a rotating exchange field is also shown for both cases. The arrows indicate the direction of the exchange field, and are placed with equidistant (center-to-center) spacing for both cases. For a curvature amplitude of  $KL = \pi/2$ , the exchange field in the corresponding straight system is oppositely aligned at the end of the wire.

ferromagnet, the best way of preserving long-ranged, spin-polarized triplets in the system is to have a region of sharp curvature near the superconducting interface for rapid conversion from short-ranged to long-ranged, and then a region of zero curvature, to avoid rotating the long-ranged components back into short-ranged triplets<sup>16</sup>. Although the conversion mechanism in this case is provided by the curvature, the process governing interconversion between components is the same as for straight multilayers with magnetic misalignment<sup>70</sup>. However, real-space curvature provides new mechanisms for design of variable exchange-field misalignment, and dynamic control of their relationship.

The utility of curvature for controlling the generation of spin-polarized superconducting correlations becomes particularly clear when considering the equivalent field of two J-curves with opposite chirality, as in Fig. 3. We see that the sign of the curvature at the superconducting interface governs the direction of the exchange field at the edge of the corresponding straight wire, which will be opposite for a curvature amplitude of  $KL = \pi/2$ . Transport through such wires will therefore experience opposite chiralities, and we can detect signatures of this chirality in the observables for superconducting correlations.

When we have a superconductor-ferromagnet-superconductor (SFS) junction instead of a bilayer, we must take into account the triplet conversion from both superconductors. Since the proximity effect at each interface will experience a chirality-dependent triplet conversion, combinations of different chiralities can therefore be expected to interfere constructively or destructively along the wire, which we explore below.

### C. C- and S-type junctions

With our knowledge of the chirality-dependent polarization of a J-type bilayer, we can now examine and contrast the effects of combining different chiralities in SFS Josephson junctions, as illustrated by the C- and S-type wires in Fig. 1. In terms of the proximity effect, a C-type junction combines *opposite* chiralities with respect to the interface of each superconductor, and the S-type combines *equal* chiralities. That is, curving the regions close to the interface rotates the exchange field to give a component perpendicular to the direction of transport in the equivalent straight case (see Fig. 3). For the C-type junction, this component points in the opposite direction near each interface, and points in the same direction for S-type. Limiting cases now give the corresponding exchange field profiles of a junction with three misaligned ferromagnets<sup>70–73</sup>, or a ferromagnet with domain walls at the interfaces<sup>10</sup>. As before, sharp curvatures at a superconducting interface promotes long-ranged triplet generation, and any further rotation along the wire will induce spin relaxation. Parametrization with the shape parameter,  $q$ , lets us vary the relative length of the straight and curved segments, and allows for separation of curvature-induced and length-induced effects.

We adopt the convention that with  $K > 0$ , we have  $\kappa(s=0) > 0$ , and the wire curves counter-clockwise at the origin (as in Fig. 2). How the proximity-induced triplets will combine in a junction will therefore depend on the radius of curvature, and any change in sign of  $K$  along the arclength. Below, we will show that the full Usadel equation predicts a chirality-dependent magnetization and spin current density in C-type junctions with constant curvature in Sec. III C 1, and go on to show the effect of constructive and destructive chirality combinations in the critical current of C- and S-type junctions in Sec. III C 2.

#### 1. Chiral signatures:

##### Magnetization and spin current density

Once we have determined the Green's function, we may determine the equilibrium spin accumulation, or proximity-induced magnetization,  $M_\mu$  in the wire in the  $\mu$  direction from<sup>74</sup>

$$M_\mu = M_0 \int_{-\infty}^{\infty} d\varepsilon \text{Tr} \{ \text{diag}(\sigma_\mu, \sigma_\mu^*) \hat{g}^K \}, \quad (21)$$

where we use the ansatz  $\hat{g}^K = (\hat{g}^R - \hat{g}^A) \tanh \frac{\beta\varepsilon}{2}$  in equilibrium. The coefficient  $M_0 = g\mu_B N_0 \Delta / 16$ , with the Landé  $g$ -factor  $g \approx 2$  for electrons,  $\mu_B$  is the Bohr magneton,  $\beta = \frac{1}{k_B T}$ , and  $N_0$  is the normal-state density of states at the Fermi-level.

To demonstrate the chiral signatures, we begin by considering the case of constant curvature in C-type junctions, with different chiralities/sign of  $K$ , as depicted in Fig. 2. We show the induced magnetization along a wire

for  $K \in (-3\pi/2, 3\pi/2)$  in Fig. 4, and see that reversing the direction of the curvature also reverses the sign of the magnetization in the normal direction in Fig. 4(b), while the tangential magnetization [Fig. 4(a)] is unchanged. This leaves a chirality-dependent, observable signature of the spin polarization. We may understand this in terms of a straight SFS-junction with a rotating exchange field, which is equivalent to a curved wire with a tangential exchange field. The curved wire and its equivalent straight exchange field is illustrated in Fig. 3. In the straight case, reversing the chirality of the exchange field rotation would reverse the spin accumulation orthogonal to the transport direction. Note that the parameter determining the chirality,  $K$ , can vary continuously, and that the response,  $M_{T,N}(s)$  varies continuously as a function of  $K$ , such that this still holds in the limit  $K \rightarrow 0$ .

The effect of the exchange field chirality also gives a signature in the spin current density  $\mathbf{J}_s^\mu$ , which is given in the  $\mu$ -direction by the Keldysh component

$$\mathbf{J}_s^\mu = \frac{\hbar N_0 D}{4} \int_{-\infty}^{\infty} d\varepsilon \text{Tr} \left\{ \text{diag}(\sigma_\mu, \sigma_\mu^*) \hat{\tau}_3 (\check{g} \partial_s \check{g})^K \right\}. \quad (22)$$

In equilibrium, we can see the contributions of the triplet components in weak proximity in the binormal component:

$$\begin{aligned} \mathbf{J}_s^B = & -\frac{\hbar N_0 D}{4} \int_{-\infty}^{\infty} d\varepsilon \text{Im} \left[ d_T \partial_s \tilde{d}_N - \tilde{d}_N \partial_s d_T + \text{t.c.} \right] \tanh \frac{\beta\varepsilon}{2} \\ & -\kappa(s) \frac{\hbar N_0 D}{2} \int_{-\infty}^{\infty} d\varepsilon \text{Im} \left[ d_T \tilde{d}_T + d_N \tilde{d}_N \right] \tanh \frac{\beta\varepsilon}{2}, \quad (23) \end{aligned}$$

where t.c. indicates the tilde conjugate of the preceding terms. The normal and tangential contributions to the spin current density are zero, since the terms couple to  $d_B$  and the derivative of  $\sigma_B$ , which give zero contribution.

By inspecting the weak proximity expression (23), we can infer that the spin current density should also change sign under reversal of  $K$ : the second term is directly odd in  $\kappa$ , and we saw from the magnetization that reversing  $K$  reverses  $d_N$  and  $\tilde{d}_N$ , which will reverse the sign of the first term. This is shown in Fig. 4(c), for a phase difference of  $\phi = \pi/2$ , where the triplet contribution is maximal. We also see a second sign change for higher curvatures, here around  $KL/\pi \approx 0.6$ , due to a  $0 - \pi$  transition<sup>16</sup>.

#### 2. Mixed chiralities in the critical charge current and ground state transitions

We can consider the combination of mixed chiralities with respect to the local superconducting interface in SFS junctions by comparing the behaviour of C- and S-type junctions with varying degrees of curvature, and will find that the triplet response to the changing spin quantization axis will interfere either constructively or destructively.

The curvature-induced  $0 - \pi$  transition for in-plane SFS junctions with constant curvature is due to the singlet-triplet conversion<sup>16</sup>. Here, we will compare the behaviour

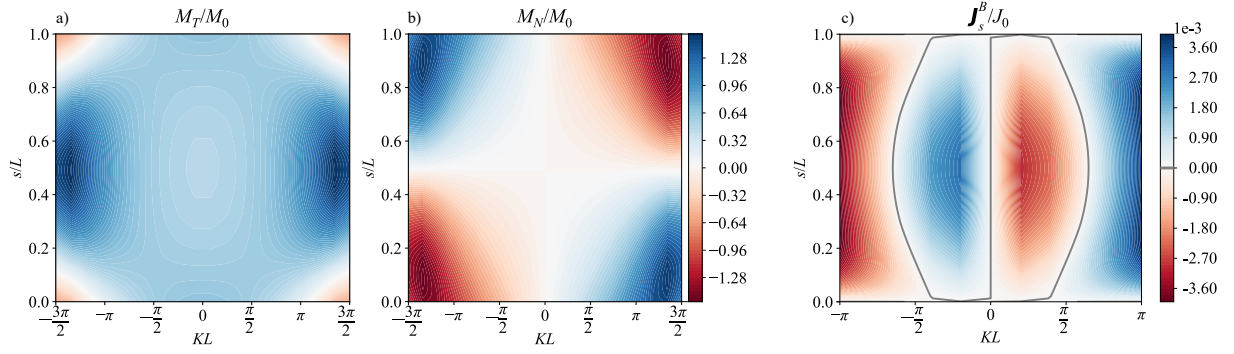


FIG. 4. Chirality-dependent signatures. Contour plots of the magnetization in the (a) tangential,  $M_T$  and (b) normal,  $M_N$  direction for an SFS junction of length  $L = 0.8\xi$ , with an exchange field of  $\mathbf{h} = \Delta\hat{T}$  as a function of arclength and constant curvature with amplitude  $KL$ . (c) Spin current density  $\mathbf{J}_s^B$  as a function of normalized position  $s/L$  for different constant curvature amplitudes  $KL$  for SFS junctions with  $L = 2\xi$ ,  $\phi = \pi/2$ ,  $T = 0.005T_c$  and  $\mathbf{h} = \Delta\hat{T}$ . The contour with  $\mathbf{J}_s^B = 0$  is traced with a thick gray line.

of junctions with mixed chiralities at the interfaces. The charge current in an SFS junction is given by the Keldysh component

$$\frac{I_Q}{I_{Q_0}} = \int_{-\infty}^{\infty} d\varepsilon \text{Tr} (\hat{\tau}_3 \check{g} \partial_s \check{g})^K, \quad (24)$$

which, in equilibrium, simplifies to

$$\frac{I_Q}{I_{Q_0}} = \int_{-\infty}^{\infty} d\varepsilon \text{Tr} \{ \hat{\tau}_3 (\hat{g}^R \partial_s \hat{g}^R - \hat{g}^A \partial_s \hat{g}^A) \} \tanh \frac{\beta\varepsilon}{2}. \quad (25)$$

Here  $I_{Q_0} = N_0 e D_F A \Delta_0 / 4L$ , where  $e$  is the electron charge,  $A$  the cross sectional area of the wire, and  $\Delta_0$  is the gap of the two identical bulk-like superconductors. The magnitude of the critical current is given in Fig. 5 as a function of the curvature amplitude  $K$ , for different ferromagnet lengths  $L$  and shapes (C, S). It is clear that here the C-type curves have a curvature-induced  $0 - \pi$  transition, whereas the S-type curves only allow for a modulation of the current.

In the case of a straight ferromagnet, the  $0 - \pi$  transition is governed by the length of the ferromagnet, due to the modulation in the acquired phase difference between the correlated spins<sup>8,75</sup>. This length-based phase acquisition is modified by the phases acquired due to curvature-induced rotation, but the length will clearly still be a factor in controlling the ground state. For example, for the parameters chosen in Fig. 5, longer junctions (e.g.  $L = 6\xi$ ) would already be in the  $\pi$  ground state for  $K = 0$ , with initial reversal of the sign of the critical current. In that case, the S-type would display a  $\pi - 0$  transition, whereas the C-type would remain in the  $\pi$ -state. We can compare the singlet and triplet contributions to the current by decomposing the anomalous Green's function

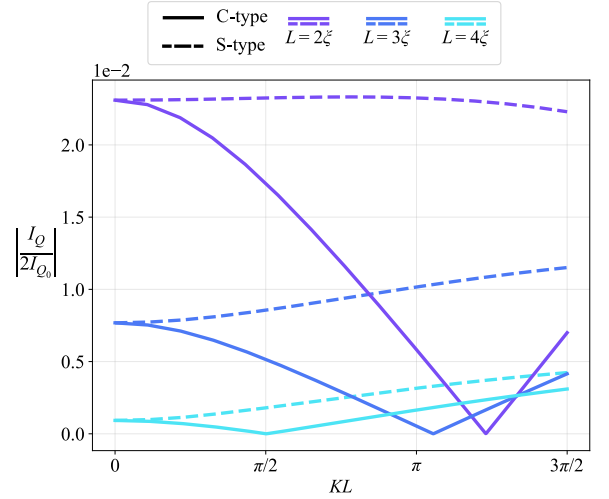


FIG. 5. Magnitude of the critical current as a function of the curvature amplitude  $K$  for different lengths  $L$  of C-type (solid line) and S-type (dashed line) with  $q/L = 0.3$  junctions.  $T = 0.005T_c$ ,  $\vec{h} = \Delta\hat{T}$ , and  $\zeta = 3$ . The C-type junctions display a curvature induced  $0 - \pi$  transition, while the S-type has none.

using Eq. (19) and writing  $I_Q/I_{Q_0} = I_0 + I_\mu + I_\kappa$ , with

$$\frac{I_0}{I_{Q_0}} = -8 \int_0^\infty d\varepsilon \text{Re} \left\{ \tilde{f}_0 \partial_s f_0 - f_0 \partial_s \tilde{f}_0 \right\} \tanh \frac{\beta\varepsilon}{2}, \quad (26a)$$

$$\frac{I_\mu}{I_{Q_0}} = +8 \int_0^\infty d\varepsilon \text{Re} \left\{ \tilde{d}_\mu \partial_s d_\mu - d_\mu \partial_s \tilde{d}_\mu \right\} \tanh \frac{\beta\varepsilon}{2}, \quad (26b)$$

$$\frac{I_\kappa}{I_{Q_0}} = 16\kappa(s) \int_0^\infty d\varepsilon \text{Re} \left\{ \tilde{d}_N d_T - \tilde{d}_T d_N \right\} \tanh \frac{\beta\varepsilon}{2} \quad (26c)$$

Here  $I_0$  represents the singlet contribution,  $I_\mu$  is the triplet contribution in the  $\mu$  direction, and  $I_\kappa$  is the inverse Edelstein contribution, present when the d-vector rotates<sup>76</sup>. That is, there will be no inverse Edelstein contribution in a straight segment of the wire here.

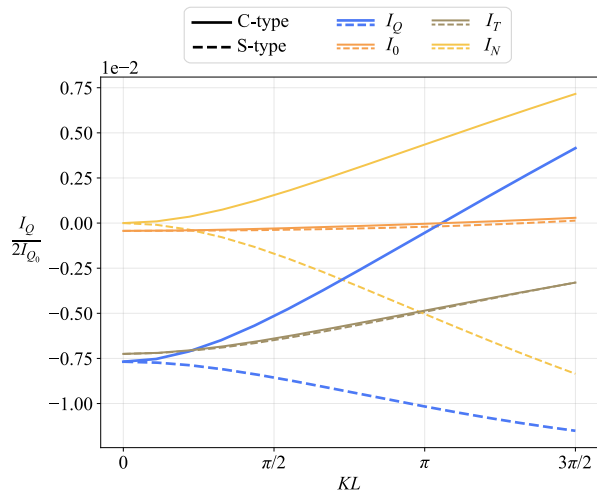


FIG. 6. The critical charge current for a C- and S-type junction, as a function of the normalized curvature amplitude  $KL$ , at  $s = L/2$  and with  $q/L = 0.3$ . The current is separated into the total,  $I_Q$ , singlet  $I_0$ , and short and long range triplet contributions,  $I_T$  and  $I_N$  respectively. Here  $L = 3\xi$ ,  $T = 0.005T_c$ ,  $\mathbf{h} = \Delta\hat{T}$ ,  $\zeta = 3$  and  $\phi = \pi/2$ . The C-type junction undergoes a  $0 - \pi$ -transition at  $KL \sim \pi$ .

As discussed above, the curvature induces generation of the long range triplet correlations by rotating the  $d$ -vector from the short ranged correlations, giving the long-range current component  $I_N$ . The first thing to notice about Fig. 6 is that  $I_N$  is almost antisymmetric with respect to the geometry being either of the S or the C type. We can understand this by employing the construction discussed in Fig. 3. By deforming the curved wire to a straight equivalent, while keeping the exchange field orientation fixed, one finds that for C-type geometries, the effective orthogonal exchange field (i.e. the component along the normal direction evaluated in the middle of the junction,  $\mathbf{h} \cdot \hat{N}(s = L/2)$ ) points in opposite directions at the ends, whereas for S-type geometries, it points in the same direction. In the former case, the  $d_N$  triplets generated at the ends, are expected to have a phase difference of  $\pi$ , which comes in addition to the Josephson effect, due to the sign change of  $h_N$ . This produces a current contribution  $I_N$  which flows in the opposite direction to the latter case, where there is no such sign-change. As we increase the curvature amplitude  $K$ , the C-type geometry therefore features a  $0 - \pi$  transition in the charge current  $I_Q$ , which is shown in Fig. 6.

#### IV. TRIPLET-SQUID DESIGN AND DISCUSSION

A triplet-SQUID design has recently been proposed for use in a superconducting memory<sup>77</sup>. It uses the conventional singlet-triplet conversion mechanism of misaligned magnetic multilayers. The two SQUID weak links are

comprised of magnetic trilayers, and the magnetization of the central layer of one link can be switched at lower field than the other. They use this to demonstrate that the ground state of a trilayer Josephson junction can switch between 0 and  $\pi$  depending on the relative magnetization of the layers<sup>70–73</sup>.

In our case, both C- and S-type curves give triplets in the middle of the ferromagnetic weak link, but only C-type gives a  $0 - \pi$  transition. This means we can achieve the same triplet-SQUID behaviour by including a ferromagnetic weak link of different curvature class in each arm of the SQUID. That is, we can use a single ferromagnetic layer for each weak link, instead of magnetic multilayer structures that are difficult to control and model accurately. Instead of needing a different sample for each new sample thickness, this design can also be parallelized by varying the planar length in parallel on the same sample. In addition, it will now be possible to switch the ground state of the junctions in-situ by employing strain, for example with electrical control via a piezoelectric substrate

In this work, we have focused on identifying signatures of different chiralities of curvilinear magnets at the interface with conventional superconductors. We chose an arbitrary shape parameter  $q$  for these demonstrations, but it would be useful to optimize the shape for maximal critical current of a junction of fixed arclength, for example.

More generally, we have shown that geometric curvature in a magnet is a versatile tool for designing bespoke effective spin-orbit coupling profiles that can vary throughout the structure. We have shown how this can be harnessed in superconducting proximity heterostructures, to control the spin polarization of superconducting correlations, giving chiral signatures in the magnetization and spin current density. When heterostructures contain multiple superconducting interfaces, the chirality at each interface should be considered in combination with the chiralities of the others. By combining elements of different chirality, as demonstrated by comparing C- and S-type junctions, we will have different mechanisms to control the ground state of the junction. We can implement this directly for improved functionality in devices, and we show how a combination of C- and S-type junctions can reproduce magnetic multi-layer triplet-SQUID behaviour.

#### ACKNOWLEDGMENTS

The computations have been performed on the SAGA supercomputer provided by UNINETT Sigma2 — the National Infrastructure for High Performance Computing and Data Storage in Norway. We acknowledge funding via the “Outstanding Academic Fellows” programme at NTNU, the “Sustainable Development Initiative” at UiO, the Research Council of Norway Grant No. 302315, as well as through its Centres of Excellence funding scheme, Project No. 262633, “Center for Quantum Spintronics”.



MA acknowledges support from the Swedish Research

Council (Grant No. VR 2019-04735 of Vladimir Juričić). Nordita is supported in part by NordForsk.

- 
- \* Corresponding author: [sol.jacobsen@ntnu.no](mailto:sol.jacobsen@ntnu.no)
- <sup>1</sup> Matthias Eschrig, “Spin-polarized supercurrents for spintronics,” *Physics Today* **64**, 43–49 (2011).
  - <sup>2</sup> Jacob Linder and Jason W. A. Robinson, “Superconducting spintronics,” *Nature Physics* **11**, 307–315 (2015).
  - <sup>3</sup> Paola Gentile, Mario Cuoco, Oleksii M. Volkov, Zu-Jian Ying, Ivan J. Vera-Marun, Denys Makarov, and Carmine Ortix, “Electronic materials with nanoscale curved geometries,” *Nature Electronics* **5**, 551–563 (2022).
  - <sup>4</sup> Tancredi Salamone, Henning G Hugdal, Morten Amundsen, and Sol H Jacobsen, “Curvature control of the superconducting proximity effect in diffusive ferromagnetic nanowires,” *Physical Review B* **105**, 134511 (2022).
  - <sup>5</sup> T. Salamone, M. Skjærpe, H. Hugdal, M. Amundsen, and S. Jacobsen, “Interface probe for antiferromagnets using geometric curvature,” [arXiv:2311.12116](https://arxiv.org/abs/2311.12116) (2023).
  - <sup>6</sup> Jacob Linder and Alexander V. Balatsky, “Odd-frequency superconductivity,” *Rev. Mod. Phys.* **91**, 045005 (2019).
  - <sup>7</sup> F. S. Bergeret, A. F. Volkov, and K. B. Efetov, “Odd triplet superconductivity and related phenomena in superconductor-ferromagnet structures,” *Rev. Mod. Phys.* **77**, 1321–1373 (2005).
  - <sup>8</sup> A. I. Buzdin, “Proximity effects in superconductor-ferromagnet heterostructures,” *Rev. Mod. Phys.* **77**, 935–976 (2005).
  - <sup>9</sup> I. F. Lyuksyutov and V. L. Pokrovsky, “Ferromagnet–superconductor hybrids,” *Advances in Physics* **54**, 67–136 (2005).
  - <sup>10</sup> F. S. Bergeret, A. F. Volkov, and K. B. Efetov, “Long-range proximity effects in superconductor-ferromagnet structures,” *Phys. Rev. Lett.* **86**, 4096–4099 (2001).
  - <sup>11</sup> J. W. A. Robinson, J. D. S. Witt, and M. G. Blamire, “Controlled injection of spin-triplet supercurrents into a strong ferromagnet,” *Science* **329**, 59–61 (2010).
  - <sup>12</sup> Trupti S. Khaire, Mazin A. Khasawneh, W. P. Pratt, and Norman O. Birge, “Observation of spin-triplet superconductivity in co-based josephson junctions,” *Phys. Rev. Lett.* **104**, 137002 (2010).
  - <sup>13</sup> F. S. Bergeret and I. V. Tokatly, “Singlet-triplet conversion and the long-range proximity effect in superconductor-ferromagnet structures with generic spin dependent fields,” *Phys. Rev. Lett.* **110**, 117003 (2013).
  - <sup>14</sup> F S Bergeret and I V Tokatly, “Spin-orbit coupling as a source of long-range triplet proximity effect in superconductor-ferromagnet hybrid structures,” *Physical Review B* **89**, 134517 (2014).
  - <sup>15</sup> Sol H Jacobsen, Jabir Ali Ouassou, and Jacob Linder, “Critical Temperature and Tunneling Spectroscopy of Superconductor-Ferromagnet Hybrids with Intrinsic Rashba–Dresselhaus Spin-Orbit Coupling,” *Physical Review B* **92**, 024510 (2015).
  - <sup>16</sup> Tancredi Salamone, Mathias B. M. Svendsen, Morten Amundsen, and Sol Jacobsen, “Curvature-induced long-range supercurrents in diffusive superconductor-ferromagnet-superconductor Josephson junctions with a dynamic  $0-\pi$  transition,” *Physical Review B* **104**, L060505 (2021).
  - <sup>17</sup> Fumiya Nagasawa, Diego Frustaglia, Henri Saarikoski, Klaus Richter, and Junsaku Nitta, “Control of the spin geometric phase in semiconductor quantum rings,” *Nature communications* **4**, 1–7 (2013).
  - <sup>18</sup> Paola Gentile, Mario Cuoco, and Carmine Ortix, “Edge states and topological insulating phases generated by curving a nanowire with rashba spin-orbit coupling,” *Phys. Rev. Lett.* **115**, 256801 (2015).
  - <sup>19</sup> Zu-Jian Ying, Paola Gentile, Carmine Ortix, and Mario Cuoco, “Designing electron spin textures and spin interferometers by shape deformations,” *Phys. Rev. B* **94**, 081406(R) (2016).
  - <sup>20</sup> Zu-Jian Ying, Mario Cuoco, Carmine Ortix, and Paola Gentile, “Tuning pairing amplitude and spin-triplet texture by curving superconducting nanostructures,” *Phys. Rev. B* **96**, 100506(R) (2017).
  - <sup>21</sup> Ching-Hao Chang and Carmine Ortix, “Theoretical prediction of a giant anisotropic magnetoresistance in carbon nanoscrolls,” *Nano letters* **17**, 3076–3080 (2017).
  - <sup>22</sup> Ari M. Turner, Vincenzo Vitelli, and David R. Nelson, “Vortices on curved surfaces,” *Rev. Mod. Phys.* **82**, 1301–1348 (2010).
  - <sup>23</sup> Gianluca Francica, Mario Cuoco, and Paola Gentile, “Topological superconducting phases and josephson effect in curved superconductors with time reversal invariance,” *Phys. Rev. B* **101**, 094504 (2020).
  - <sup>24</sup> A. G. Kutlin and A. S. Mel’nikov, “Geometry-dependent effects in majorana nanowires,” *Phys. Rev. B* **101**, 045418 (2020).
  - <sup>25</sup> Po-Hao Chou, Chia-Hsin Chen, Shih-Wei Liu, Chung-Hou Chung, and Chung-Yu Mou, “Geometry-induced topological superconductivity,” *Phys. Rev. B* **103**, 014508 (2021).
  - <sup>26</sup> G. Cantele, D. Ninno, and G. Iadonisi, “Topological surface states in deformed quantum wires,” *Phys. Rev. B* **61**, 13730–13736 (2000).
  - <sup>27</sup> H. Aoki, M. Koshino, D. Takeda, H. Morise, and K. Kuroki, “Electronic structure of periodic curved surfaces: Topological band structure,” *Phys. Rev. B* **65**, 035102 (2001).
  - <sup>28</sup> Mario Encinosa and Lonnie Mott, “Curvature-induced toroidal bound states,” *Phys. Rev. A* **68**, 014102 (2003).
  - <sup>29</sup> Carmine Ortix and Jeroen van den Brink, “Effect of curvature on the electronic structure and bound-state formation in rolled-up nanotubes,” *Phys. Rev. B* **81**, 165419 (2010).
  - <sup>30</sup> Denis D. Sheka, Oleksandr V. Pylypovskiy, Pedro Landeros, Yuri Gaididei, Attila Kákay, and Denys Makarov, “Nonlocal chiral symmetry breaking in curvilinear magnetic shells,” *Communications Physics* **3**, 128 (2020).
  - <sup>31</sup> Jae-Seung Jeong, Jeongkyu Shin, and Hyun-Woo Lee, “Curvature-induced spin-orbit coupling and spin relaxation in a chemically clean single-layer graphene,” *Phys. Rev. B* **84**, 195457 (2011).
  - <sup>32</sup> Paola Gentile, Mario Cuoco, and Carmine Ortix, “Curvature-induced Rashba spin-orbit interaction in strain-driven nanostructures,” *Spin* **3**, 1340002 (2013).
  - <sup>33</sup> Yong-Long Wang, Hua Jiang, and Hong-Shi Zong, “Geometric influences of a particle confined to a curved surface embedded in three-dimensional euclidean space,” *Phys. Rev.*

- A **96**, 022116 (2017).
- <sup>34</sup> Robert Streubel, Peter Fischer, Florian Kronast, Volodymyr P. Kravchuk, Denis D. Sheka, Yuri Gaididei, Oliver G. Schmidt, and Denys Makarov, “Magnetism in curved geometries,” *Journal of Physics D: Applied Physics* **49**, 363001 (2016).
- <sup>35</sup> Denis D. Sheka, “A perspective on curvilinear magnetism,” *Applied Physics Letters* **118**, 230502 (2021).
- <sup>36</sup> Robert Streubel, Evgeny Y. Tsybmal, and Peter Fischer, “Magnetism in curved geometries,” *Journal of Applied Physics* **129**, 210902 (2021).
- <sup>37</sup> Hiroshi Imamura, Patrick Bruno, and Yasuhiro Utsumi, “Twisted exchange interaction between localized spins embedded in a one- or two-dimensional electron gas with rashba spin-orbit coupling,” *Phys. Rev. B* **69**, 121303(R) (2004).
- <sup>38</sup> Kyoung-Whan Kim, Hyun-Woo Lee, Kyung-Jin Lee, and M. D. Stiles, “Chirality from interfacial spin-orbit coupling effects in magnetic bilayers,” *Phys. Rev. Lett.* **111**, 216601 (2013).
- <sup>39</sup> A. Kundu and S. Zhang, “Dzyaloshinskii-moriya interaction mediated by spin-polarized band with rashba spin-orbit coupling,” *Phys. Rev. B* **92**, 094434 (2015).
- <sup>40</sup> Yuri Gaididei, Volodymyr P. Kravchuk, and Denis D. Sheka, “Curvature effects in thin magnetic shells,” *Phys. Rev. Lett.* **112**, 257203 (2014).
- <sup>41</sup> Smiljan Vojkovic, Vagson L. Carvalho-Santos, Jakson M. Fonseca, and Álvaro S. Núñez, “Vortex-antivortex pairs induced by curvature in toroidal nanomagnets,” *Journal of Applied Physics* **121**, 113906 (2017).
- <sup>42</sup> A. W. Teixeira, S. Castillo-Sepúlveda, S. Vojkovic, J. M. Fonseca, D. Altbir, Á. S. Núñez, and V. L. Carvalho-Santos, “Analysis on the stability of in-surface magnetic configurations in toroidal nanoshells,” *Journal of Magnetism and Magnetic Materials* **478**, 253–259 (2019).
- <sup>43</sup> J. A. Otálora, J. A. López-López, P. Vargas, and P. Landeros, “Chirality switching and propagation control of a vortex domain wall in ferromagnetic nanotubes,” *Applied Physics Letters* **100**, 072407 (2012).
- <sup>44</sup> D. Mancilla-Almonacid, M.A. Castro, J.M. Fonseca, D. Altbir, S. Allende, and V.L. Carvalho-Santos, “Magnetic ground states for bent nanotubes,” *Journal of Magnetism and Magnetic Materials* **507**, 166754 (2020).
- <sup>45</sup> V.L. Carvalho-Santos, F.A. Apolonio, and N.M. Oliveira-Neto, “On geometry-dependent vortex stability and topological spin excitations on curved surfaces with cylindrical symmetry,” *Physics Letters A* **377**, 1308–1316 (2013).
- <sup>46</sup> Oleksii M. Volkov, Denis D. Sheka, Yuri Gaididei, Volodymyr P. Kravchuk, Ulrich K. Rößler, Jürgen Fassbender, and Denys Makarov, “Mesoscale dzyaloshinskii-moriya interaction: geometrical tailoring of the magnetochirality,” *Scientific Reports* **8**, 866 (2018).
- <sup>47</sup> Oleksandr V. Pylypovskiy, Denys Y. Kononenko, Kostiantyn V. Yershov, Ulrich K. Rößler, Artem V. Tomilo, Jürgen Fassbender, Jeroen van den Brink, Denys Makarov, and Denis D. Sheka, “Curvilinear one-dimensional antiferromagnets,” *Nano Letters* **20**, 8157–8162 (2020).
- <sup>48</sup> Volodymyr P. Kravchuk, Denis D. Sheka, Robert Streubel, Denys Makarov, Oliver G. Schmidt, and Yuri Gaididei, “Out-of-surface vortices in spherical shells,” *Phys. Rev. B* **85**, 144433 (2012).
- <sup>49</sup> Denis D Sheka, Volodymyr P Kravchuk, and Yuri Gaididei, “Curvature effects in statics and dynamics of low dimensional magnets,” *Journal of Physics A: Mathematical and Theoretical* **48**, 125202 (2015).
- <sup>50</sup> Oliver G Schmidt and Karl Eberl, “Thin solid films roll up into nanotubes,” *Nature* **410**, 168–168 (2001).
- <sup>51</sup> P. Cendula, S. Kiravittaya, Y. F. Mei, Ch. Deneke, and O. G. Schmidt, “Bending and wrinkling as competing relaxation pathways for strained free-hanging films,” *Phys. Rev. B* **79**, 085429 (2009).
- <sup>52</sup> Sheng Xu, Zheng Yan, Kyung-In Jang, Wen Huang, Hao-ran Fu, Jeonghyun Kim, Zijun Wei, Matthew Flavin, Joselle McCracken, Renhan Wang, Adina Badea, Yuhao Liu, Dongqing Xiao, Guoyan Zhou, Jungwoo Lee, Ha Uk Chung, Huanyu Cheng, Wen Ren, Anthony Banks, Xiuling Li, Ungyu Paik, Ralph G. Nuzzo, Yonggang Huang, Yihui Zhang, and John A. Rogers, “Assembly of micro/nanomaterials into complex, three-dimensional architectures by compressive buckling,” *Science* **347**, 154–159 (2015).
- <sup>53</sup> E. R. Lewis, D. Petit, L. Thevenard, A. V. Jausovec, L. O’Brien, D. E. Read, and R. P. Cowburn, “Magnetic domain wall pinning by a curved conduit,” *Applied Physics Letters* **95**, 152505 (2009).
- <sup>54</sup> D. M. Burn, M. Chadha, S. K. Walton, and W. R. Branford, “Dynamic interaction between domain walls and nanowire vertices,” *Phys. Rev. B* **90**, 144414 (2014).
- <sup>55</sup> Oleksii M. Volkov, Attila Kákay, Florian Kronast, Ingolf Mönch, Mohamad-Assaad Mawass, Jürgen Fassbender, and Denys Makarov, “Experimental observation of exchange-driven chiral effects in curvilinear magnetism,” *Phys. Rev. Lett.* **123**, 077201 (2019).
- <sup>56</sup> Gwilym Williams, Matthew Hunt, Benedikt Boehm, Andrew May, Michael Taverne, Daniel Ho, Sean Giblin, Dan Read, John Rarity, Rolf Allenspach, and Sam Ladak, “Two-photon lithography for 3d magnetic nanostructure fabrication,” *Nano Research* **11**, 845–854 (2018).
- <sup>57</sup> Joseph Askey, Matthew Oliver Hunt, Wolfgang Langbein, and Sam Ladak, “Use of two-photon lithography with a negative resist and processing to realise cylindrical magnetic nanowires,” *Nanomaterials* **10** (2020), 10.3390/nano10030429.
- <sup>58</sup> B. Dick, M. J. Brett, T. J. Smy, M. R. Freeman, M. Malac, and R. F. Egerton, “Periodic magnetic microstructures by glancing angle deposition,” *Journal of Vacuum Science & Technology A* **18**, 1838–1844 (2000).
- <sup>59</sup> Dédalo Sanz-Hernández, Aurelio Hierro-Rodriguez, Claire Donnelly, Javier Pablo-Navarro, Andrea Sorrentino, Eva Pereiro, César Magén, Stephen McVitie, José María de Teresa, Salvador Ferrer, Peter Fischer, and Amalio Fernández-Pacheco, “Artificial double-helix for geometrical control of magnetic chirality,” *ACS Nano* **14**, 8084–8092 (2020).
- <sup>60</sup> O. V. Dobrovolskiy, N. R. Vovk, A. V. Bondarenko, S. A. Bunyaev, S. Lamb-Camarena, N. Zenbaa, R. Sachser, S. Barth, K. Y. Guslienko, A. V. Chumak, M. Huth, and G. N. Kakazei, “Spin-wave eigenmodes in direct-write 3D nanovolcanoes,” *Applied Physics Letters* **118**, 132405 (2021).
- <sup>61</sup> B. Kundys, “Photostrictive materials,” *Applied Physics Reviews* **2**, 011301 (2015).
- <sup>62</sup> Sylvia Matzen, Loïc Guillemot, Thomas Maroutian, Sheena K. K. Patel, Haidan Wen, Anthony D. DiChiara, Guillaume Agnus, Oleg G. Shpyrko, Eric E. Fullerton, Dafiné Ravelosona, Philippe Lecoeur, and Roopali Kukreja, “Tuning ultrafast photoinduced strain in ferroelectric-based devices,” *Advanced Electronic Materials* **5**, 1800709 (2019).

- <sup>63</sup> Lilian Guillemany, Laurent Lermusiaux, Guillaume Landaburu, Benoit Wagnon, and Benjamin Abécassis, “Curvature and self-assembly of semi-conducting nanoplatelets,” *Communications Chemistry* **5**, 7 (2022).
- <sup>64</sup> Wolfgang Belzig, Frank K Wilhelm, Christoph Bruder, Gerd Schön, and Andrei D Zaikin, “Quasiclassical green’s function approach to mesoscopic superconductivity,” *Superlattices and Microstructures* **25**, 1251–1288 (1999).
- <sup>65</sup> Klaus D. Usadel, “Generalized diffusion equation for superconducting alloys,” *Phys. Rev. Lett.* **25**, 507–509 (1970).
- <sup>66</sup> Carmine Ortix, “Quantum mechanics of a spin-orbit coupled electron constrained to a space curve,” *Physical Review B* **91**, 245412 (2015).
- <sup>67</sup> M Yu Kuprianov and VF Lukichev, “Influence of boundary transparency on the critical current of dirty ss’s structures,” *Zh. Eksp. Teor. Fiz* **94**, 149 (1988).
- <sup>68</sup> Nils Schopohl and Kazumi Maki, “Quasiparticle spectrum around a vortex line in a d-wave superconductor,” *Phys. Rev. B* **52**, 490–493 (1995).
- <sup>69</sup> Jabir Ali Ouassou, “*Geneus*,” (2018).
- <sup>70</sup> M. Houzet and A. I. Buzdin, “Long range triplet josephson effect through a ferromagnetic trilayer,” *Phys. Rev. B* **76**, 060504 (2007).
- <sup>71</sup> A. F. Volkov, F. S. Bergeret, and K. B. Efetov, “Odd triplet superconductivity in superconductor-ferromagnet multilayered structures,” *Phys. Rev. Lett.* **90**, 117006 (2003).
- <sup>72</sup> A. F. Volkov and K. B. Efetov, “Odd spin-triplet superconductivity in a multilayered superconductor-ferromagnet josephson junction,” *Phys. Rev. B* **81**, 144522 (2010).
- <sup>73</sup> Luka Trifunovic and Zoran Radović, “Long-range spin-triplet proximity effect in josephson junctions with multilayered ferromagnets,” *Phys. Rev. B* **82**, 020505 (2010).
- <sup>74</sup> T. Champel and M. Eschrig, “Effect of an inhomogeneous exchange field on the proximity effect in disordered superconductor-ferromagnet hybrid structures,” *Phys. Rev. B* **72**, 054523 (2005).
- <sup>75</sup> T. Kontos, M. Aprili, J. Lesueur, F. Genêt, B. Stephanidis, and R. Boursier, “Josephson junction through a thin ferromagnetic layer: Negative coupling,” *Phys. Rev. Lett.* **89**, 137007 (2002).
- <sup>76</sup> Morten Amundsen and Jacob Linder, “Supercurrent vortex pinball via a triplet Cooper pair inverse Edelstein effect,” *Physical Review B* **96**, 064508 (2017).
- <sup>77</sup> Joseph A. Glick, Victor Aguilar, Adel B. Gougam, Bethany M. Niedzielski, Eric C. Gingrich, Reza Loloee, William P. Pratt, and Norman O. Birge, “Phase control in a spin-triplet squid,” *Science Advances* **4**, eaat9457 (2018).